Quantitative Label-Free Imaging of 3D Vascular Networks Self-Assembled in Synthetic Hydrogels

HHS Public Access

Author manuscript

Adv Healthc Mater. Author manuscript; available in PMC 2019 July 01.

Published in final edited form as:

Adv Healthc Mater. 2019 January ; 8(2): e1801186. doi:10.1002/adhm.201801186.

Quantitative Label-Free Imaging of 3D Vascular Networks Self-Assembled in Synthetic Hydrogels

Gaurav Kaushik,
Human Models for Analysis of Pathways (HMAPs) Center, University of Wisconsin—Madison, 1111 Highland Avenue, WIMR 5418, Madison, WI 53705, USA

Department of Orthopedics and Rehabilitation, University of Wisconsin—Madison, 1111 Highland Avenue, WIMR 5418, Madison, WI 53705, USA

Daniel A. Gil,
Department of Biomedical Engineering, University of Wisconsin—Madison, 1415 Engineering Drive, Madison, WI 53706, USA

Morgridge Institute for Research, 330 North Orchard Street, Madison, WI 53715, USA

Elizabeth Torr,
Human Models for Analysis of Pathways (HMAPs) Center, University of Wisconsin—Madison, 1111 Highland Avenue, WIMR 5418, Madison, WI 53705, USA

Department of Orthopedics and Rehabilitation, University of Wisconsin—Madison, 1111 Highland Avenue, WIMR 5418, Madison, WI 53705, USA

Elizabeth S. Berge,
Department of Biomedical Engineering, University of Wisconsin—Madison, 1415 Engineering Drive, Madison, WI 53706, USA

Morgridge Institute for Research, 330 North Orchard Street, Madison, WI 53715, USA

Cheryl Soref,
Human Models for Analysis of Pathways (HMAPs) Center, University of Wisconsin—Madison, 1111 Highland Avenue, WIMR 5418, Madison, WI 53705, USA

Department of Orthopedics and Rehabilitation, University of Wisconsin—Madison, 1111 Highland Avenue, WIMR 5418, Madison, WI 53705, USA

Peyton Uhl,
Human Models for Analysis of Pathways (HMAPs) Center, University of Wisconsin—Madison, 1111 Highland Avenue, WIMR 5418, Madison, WI 53705, USA

Department of Orthopedics and Rehabilitation, University of Wisconsin—Madison, 1111 Highland Avenue, WIMR 5418, Madison, WI 53705, USA

william.daly@wisc.edu; wlmurphy@wisc.edu.

Conflict of Interest
The authors declare no conflict of interest.

Supporting Information
Supporting Information is available from the Wiley Online Library or from the author.

Gianluca Fontana,
Human Models for Analysis of Pathways (HMAPs) Center, University of Wisconsin—Madison, 1111 Highland Avenue, WIMR 5418, Madison, WI 53705, USA

Department of Orthopedics and Rehabilitation, University of Wisconsin—Madison, 1111 Highland Avenue, WIMR 5418, Madison, WI 53705, USA

Jessica Antosiewicz-Bourget,
Morgridge Institute for Research, 330 North Orchard Street, Madison, WI 53715, USA

Human Models for Analysis of Pathways (HMAPs) Center, University of Wisconsin—Madison, 1111 Highland Avenue, WIMR 5418, Madison, WI 53705, USA

Collin Edington,
Department of Biological Engineering, Massachusetts Institute of Technology, 77 Massachusetts Avenue, Cambridge, MA 02139, USA

Michael P. Schwartz,
Department of Biomedical Engineering, University of Wisconsin—Madison, 1415 Engineering Drive, Madison, WI 53706, USA

Linda G. Griffith,
Department of Biological Engineering, Massachusetts Institute of Technology, 77 Massachusetts Avenue, Cambridge, MA 02139, USA

James A. Thomson,
Morgridge Institute for Research, 330 North Orchard Street, Madison, WI 53715, USA

Human Models for Analysis of Pathways (HMAPs) Center, University of Wisconsin—Madison, 1111 Highland Avenue, WIMR 5418, Madison, WI 53705, USA

Melissa C. Skala,
Department of Biomedical Engineering, University of Wisconsin—Madison, 1415 Engineering Drive, Madison, WI 53706, USA

Morgridge Institute for Research, 330 North Orchard Street, Madison, WI 53715, USA

Human Models for Analysis of Pathways (HMAPs) Center, University of Wisconsin—Madison, 1111 Highland Avenue, WIMR 5418, Madison, WI 53705, USA

William T. Daly, and
Human Models for Analysis of Pathways (HMAPs) Center, University of Wisconsin—Madison, 1111 Highland Avenue, WIMR 5418, Madison, WI 53705, USA

Department of Orthopedics and Rehabilitation, University of Wisconsin—Madison, 1111 Highland Avenue, WIMR 5418, Madison, WI 53705, USA

William L. Murphy
Department of Biomedical Engineering, University of Wisconsin—Madison, 1415 Engineering Drive, Madison, WI 53706, USA

Human Models for Analysis of Pathways (HMAPs) Center, University of Wisconsin—Madison, 1111 Highland Avenue, WIMR 5418, Madison, WI 53705, USA

Department of Orthopedics and Rehabilitation, University of Wisconsin—Madison, 1111 Highland Avenue, WIMR 5418, Madison, WI 53705, USA

Abstract

Vascularization is an important strategy to overcome diffusion limits and enable the formation of complex, physiologically relevant engineered tissues and organoids. Self-assembly is a technique to generate in vitro vascular networks, but engineering the necessary network morphology and function remains challenging. Here, autofluorescence multiphoton microscopy (aMPM), a label-free imaging technique, is used to quantitatively evaluate in vitro vascular network morphology. Vascular networks are generated using human embryonic stem cell–derived endothelial cells and primary human pericytes encapsulated in synthetic poly(ethylene glycol)-based hydrogels. Two custom-built bioreactors are used to generate distinct fluid flow patterns during vascular network formation: recirculating flow or continuous flow. aMPM is used to image these 3D vascular networks without the need for fixation, labels, or dyes. Image processing and analysis algorithms are developed to extract quantitative morphological parameters from these label-free images. It is observed with aMPM that both bioreactors promote formation of vascular networks with lower network anisotropy compared to static conditions, and the continuous flow bioreactor induces more branch points compared to static conditions. Importantly, these results agree with trends observed with immunocytochemistry. These studies demonstrate that aMPM allows label-free monitoring of vascular network morphology to streamline optimization of growth conditions and provide quality control of engineered tissues.

Keywords

autofluorescence; multiphoton microscopy; poly(ethylene glycol); self-assembly; vascular networks

1. Introduction

3D engineered tissues generated from pluripotent stem cells are a powerful tool to model human development and disease in a dish.[1] However, the size and complexity of these tissues are currently restricted by the diffusion limit, which causes cells deeper than ≈200 μm to experience insufficient nutrient and waste exchange, leading to cell death or dysfunction.[2–4] Vascularization can improve mass transport and enable growth of thick, complex engineered tissues.[5] Many approaches to generate vascular networks have been demonstrated, including microfabrication,[6,7] sacrificial templating,[8] bioprinting,[3,9] microfluidic devices,[1,10–12] and self-assembly.[13,14] Self-assembly relies on the self-organization of endothelial and mural cells (i.e., pericytes and vascular smooth muscle cells) into vascular networks. We recently demonstrated that poly(ethylene glycol) (PEG) hydrogels engineered to mimic the extracellular matrix support self-assembled vascular network formation.[7,10,15–17]

The relative simplicity of self-assembly makes it uniquely adaptable and scalable for producing engineered tissue, but inherently lacks precise control over the final morphology of the network. Thus, achieving the desired network morphology requires iteration between

adjusting growth conditions and imaging the subsequent network morphology. However, current methods to assess vascular network morphology are limited. Common immunocytochemistry protocols only capture network morphology at a single time point and use fixatives (e.g., formalin) that can distort vascular network morphology.[18] Fluorescent protein expression or live fluorescent dyes enable live-cell imaging, but some fluorophores cause oxidative stress or phototoxicity,[19] and such labels cannot be used in samples destined for human transplant. We hypothesized that label-free imaging could be used to visualize the morphology of vascular networks, which would avoid fixation, dyes, or labels.

Here, we demonstrate autofluorescence multiphoton microscopy (aMPM) of self-assembled in vitro vascular networks. In this study, aMPM exploits the fluorescence of reduced nicotinamide adenine dinucleotide and reduced nicotinamide adenine dinucleotide phosphate, jointly referred to as NAD(P)H, which are endogenous coenzymes for metabolic reactions in the cell.[20] aMPM, and more generally MPM, uses near-infrared excitation wavelengths that are well suited to evaluate thick in vitro models due to reduced scattering of the excitation wavelengths compared to confocal microscopy.[21] Although NAD(P)H fluorescence is weak compared to exogenous fluorophores, MPM has imaged NAD(P)H across a wide range of in vitro and in vivo samples.[20,22] Here, MPM enabled quantitative analysis of multiple relevant vascular network parameters, including vessel diameter, branch point density, and network anisotropy (i.e., vessel alignment).

Additionally, we were interested in visualizing and determining the change in vascular network morphology and interconnectivity in the presence of dynamic flow.[1] Fluid flow plays a key role during in vivo blood vessel development, and dynamic flow has been successfully applied in microfluidic devices to generate stable and perfusable vascular networks via increased sprout formation,[12] capillary development,[23] and endothelial cell migration.[24] We explored two bioreactors with distinct flow patterns: i) a recirculating flow bioreactor, which generated recirculating flow in the basal media below the developing vascular networks in each well (18 vascular networks per device); and ii) a continuous flow bioreactor, which applied unidirectional flow that constantly refreshed the media in each well (6 vascular networks per device). We believed that dynamic flow would induce the formation of multiscale, interconnected vascular networks that are stable over time, like in vivo vasculature.[23–25]

Our results confirm that human embryonic stem cell (ESC)-derived endothelial cells (ECs) and primary human pericytes cultured in PEG hydrogels self-assemble into 3D vascular networks under both static and dynamic flow conditions. aMPM monitored in vitro vascular network morphology without fixation or labels and observed trends similar to standard immunocytochemistry. Dynamic flow conditions improved the interconnectivity of self-assembled vascular networks. Collectively, these results will impact efforts to vascularize engineered tissue, screen angiogenic compounds for drug discovery and toxin identification,[15,26] and understand vascular tissue development[27] and disease.[28]

2. Results

2.1. Vascular Network Characterization

Vascular networks self-assembled in PEG hydrogels under static (Figure 1C) and dynamic (Figure 1A–C) flow conditions. At day 6, EC ($CD31^+$ and VE-$cadherin^+$) and pericyte ($PDGFR\beta^+$ and αSMA^+) markers were expressed throughout the vascular network in all culture conditions (Figure 2A; Figure S1, Supporting Information). Further, as tight junctions are a standard feature of blood vessels, we also stained vascular networks cultured under static conditions for the tight junction marker zonula occludens-1 (ZO-1) and the cell adhesion molecule VE-cadherin (Figure S2, Supporting Information).[29] ZO-1 was expressed in a punctate manner along the edges of each vessel, while VE-cadherin was more uniformly expressed throughout the vessels. Notably, many ECs ($CD31^+$ cells) were also suspended in the hydrogel and not integrated into the vascular networks. Scanning electron microscopy (SEM) images of the vascular network showed pericytes wrapped around apparent EC lumens (Figure 2B). A rendering of an aMPM volume showed the 3D morphology of the vascular networks (Figure 2C).

2.2. Segmentation and Quantification of Vascular Network Morphology

An image processing pipeline was developed to segment aMPM images of self-assembled vascular networks. The pipeline (Figure 3) segmented free cells and the vascular network, which has a low, spatially varying signal-to-background ratio (SBR). Segmentation and removal of free cells was achieved based on their distinctive size and morphology (i.e., eccentricity and circularity) compared to the vascular network. The SBR of the vascular networks was improved via a two-step procedure of contrast-limited adaptive histogram equalization (CLAHE), which locally enhances contrast, followed by multiscale Hessian filtering, which enhances vessel-like structures and suppresses background regions. The performance of this pipeline was quantified using the Sørensen-Dice similarity coefficient, which assesses the correspondence of two binary masks. A representative comparison can be seen in Figure S3B in the Supporting Information. Here, we compared masks generated automatically through the image processing pipeline to their corresponding manually segmented binary mask and found our pipeline yielded Sørensen-Dice similarity coefficients of 0.828, 0.834, and 0.844 across three representative mask pairs (automated and manual). The masks generated from our pipeline were used to quantify the five morphological parameters illustrated in Figure 4: vessel diameter, vascular density, branch point density, free/networked ratio, and network anisotropy.

2.3. aMPM Quantification of Live Vascular Network Morphology

Dynamic culture conditions in both recirculating and continuous flow bioreactors induced differences in vascular network morphology compared to the static condition (Figure 5A). The image processing pipeline enabled measurement of quantitative morphological parameters (Figure 5B–G). No change was observed in mean vessel diameter, vascular density, and free/networked ratio between different culture conditions (Figure 5C–E). The continuous flow bioreactor increased branch point density compared to static conditions (Figure 5F). Both the recirculating flow and continuous flow bioreactors significantly decreased network anisotropy compared to static conditions, and the continuous flow

bioreactor significantly decreased network anisotropy compared to the recirculating flow bioreactor (Figure 5G). The histogram of vessel diameters pooled across all aMPM data is shown in Figure S4 in the Supporting Information.

2.4. Confocal Quantification of Fixed Vascular Network Morphology

The image processing pipeline was applied to images of immunocytochemistry and showed similar trends to those observed using aMPM (Figure 6). No change was observed in mean vessel diameter, vascular density, and free/networked ratio between different culture conditions (Figure 6C–E). Both the recirculating flow and continuous flow bioreactors significantly increased branch point density when compared to static conditions, and the continuous flow bioreactor significantly increased branch point density compared to the recirculating flow bioreactor (Figure 6F). The continuous flow bioreactor also significantly decreased network anisotropy compared to static conditions (Figure 6G). The histogram of vessel diameters pooled across all immunocytochemistry data is shown in Figure S4 in the Supporting Information.

3. Discussion and Conclusion

Engineered tissues and organoids are restricted in size, function, and viability by diffusion-limited mass transport.[30] Nutrient and oxygen gradients due to limited mass transport can cause undesirable phenotypic adaptations (e.g., for hypoxia or nutrient starvation) or cell death (i.e., necrotic core formation).[31] Vascularization is an important strategy to improve mass transport and enable large, complex engineered tissues and organoids.[2] Generally, this is achieved through prevascularization, which involves generating a vascular network and then seeding the cells necessary for the desired tissue type. Self-assembly is an established method to generate in vitro vascular networks and relies on self-organization of endothelial cells and mural cells into vessel-like structures when cocultured in a 3D environment.[10,13,14,16,32] Overall, self-assembly is an attractive technique for generating vascular networks because of its simplicity and scalability, which could enable high-throughput generation of vascular networks. However, self-assembly inherently lacks control over the network morphology, and there are no optimal culture conditions identified to date for assembly of in vivo-like vascular networks. Here, we demonstrated aMPM, a label-free imaging technique, to quantitatively evaluate vascular network morphology and applied this label-free imaging technique to assess the effect of dynamic culture conditions on self-assembled vascular network morphology.

First, we confirmed that ECs and pericytes self-assembled together to form vascular network under static and dynamic flow conditions. Previous studies have shown that the cross-talk between pericytes and ECs is vital for self-assembly of in vitro vascular networks.[33] Standard immunocytochemistry markers for ECs (CD31, VE-cadherin) and pericytes (PDGFRβ, αSMA) were imaged using confocal microscopy, which allowed us to visualize the colocalization of ECs with pericytes along the vessel lumen. In addition, we observed punctate expression of tight junction marker ZO-1 along the vessel walls, which suggests that the vascular networks are still immature and lack barrier function (i.e., leaky vessels) at day 6.[34–36] This is unsurprising, as early vascular remodeling and pruning processes were

presumably involved during the formation of vascular networks, and the vascular network did not mature fully during the time frame of these experiments.[36]

aMPM represents a novel method to visualize vascular network morphology without labels. aMPM images of vascular networks in our study generally had low signal-to-background ratios, which we attribute to the low quantum yield of NAD(P) H and limited amount of cellular material that make up each vessel in the vascular network. Accurate segmentation of the 2D maximum intensity projections (MIPs) was critical, since the parameters to quantify vascular network morphology are extracted based on segmented MIPs. Our image processing pipeline accurately segments the vascular networks by combining background subtraction, local contrast enhancement using CLAHE, and multiscale Hessian filtering to enhance vascular structures across scales and suppress background regions. Unlike immunocytochemistry, aMPM offers the potential for real-time monitoring of network formation. aMPM also avoids the need for exogenous fluorophores that may not be appropriate for all tissue engineering applications (e.g., toxicology, quality control of engineered tissue for therapy). Additionally, aMPM can extract cell-level information on the health of the vascular network by exploiting redox imaging and fluorescence lifetime imaging microscopy of endogenous fluorophores, NAD(P)H and flavin adenine dinucleotide, which are involved in cellular metabolism.[20,22] This approach has been used by a number of groups to assess the structure, function, and metabolism of engineered tissues.[37] aMPM provides labelfree visualization of engineered tissues but includes some limitations. First, cellular autofluorescence is weak, so substrate materials with low autofluorescence are ideal (e.g., PEG hydrogels). Additionally, two-photon fluorescence of NAD(P)H is generally limited to depths of ≈500 μm, but greater imaging depths could be achieved with three-photon excitation.[38]

We quantitatively assessed the effect of static, recirculating flow, and continuous flow conditions on vascular network morphology with both aMPM of live vascular networks and confocal microscopy of fixed vascular networks. Notably, while some parameters extracted from aMPM and confocal images had different absolute values (Figures 5 and 6; Figure S4, Supporting Information), we observed similar trends across all morphological parameters. We attribute the difference in absolute values to the dehydration and shrinkage of the PEG hydrogel caused by the standard immunocytochemistry fixation process (4% paraformaldehyde (PFA)).[18] The variability between experimental samples was inherent to self-assembly and the culture process. We found that dynamic flow conditions induced vascular networks with different morphology than those cultured in static conditions. Specifically, we observed with aMPM that vascular networks cultured in the continuous flow bioreactor showed significantly more branch points than samples in static conditions and lower network anisotropy than samples in both static conditions and the recirculating flow bioreactor. Together, these morphological differences could indicate the formation of a more interconnected vascular network induced by the increased biomechanical stimulation provided by the bioreactor.[12,35,39] In contrast, the aMPM data showed that samples cultured in the recirculating flow bioreactor had significantly lower network anisotropy but no change in branch points from control. While additional studies are needed to understand these differences in anisotropy, our results demonstrate that aMPM provides a valuable tool

for quantifying how conditions such as varying flow profiles impact vascular network formation.

Improvements in aMPM technology that increase imaging speed (e.g., two-photon light sheet microscopy) would enable future studies to noninvasively monitor vascular network formation.[40] Additional improvements in image processing and analysis methods would allow us to directly quantify 3D aMPM volumes rather than 2D MIPs.[41] Lastly, more bioreactors compatible with microscopy are needed to understand the role of biophysical signaling on vascular network development.[42] Ultimately, this technology may be applied to explore the link between vascular network morphology and the function and viability of vascularized organoids.

4. Experimental Section

Cell Culture and Maintenance—Media Formulations—Essential 7 V (E7V) Medium

DMEM/F12 HEPES (Thermo Fisher Scientific, Madison, WI), L-ascorbic acid-2-phosphate magnesium (64 mg L^{-1}; Sigma-Aldrich, A8960–5G), sodium selenite (14 μg L^{-1}; Sigma-Aldrich, S5261), $NaHCO_3$ (543 mg L^{-1}), holo-transferrin (10.7 mg L^{-1}; Sigma-Aldrich, T0665–1G), insulin (20 mg L^{-1}; Sigma-Aldrich, I9278), human recombinant FGF2 (100 μg L^{-1}), and vascular endothelial growth factor A (VEGF-A; 50 μg L^{-1}).

Cell Culture and Maintenance—Media Formulations—Pericyte Medium

The pericyte medium was prepared by adding 10 mL of fetal bovine serum (ScienCell Research Laboratories, Carlsbad, CA) and 5 mL of pericyte growth supplement (ScienCell Research Laboratories, Carlsbad, CA) into 500 mL basal medium (ScienCell Research Laboratories, Carlsbad, CA).

Cell Culture and Maintenance—Endothelial Cell Differentiation and Pericyte Cell Culture

Endothelial cells were generated from H1 ESCs using a previously reported protocol with some modifications.[17] Briefly, ESCs were cultured on Matrigel-coated plates (Corning, New York) with E8 medium (Thermo Fisher Scientific, Madison, WI) and passaged with 0.5 × 10^{-3} m ethylenediaminetetraacetic acid in 0.01 m phosphate-buffered saline without calcium and magnesium (PBS). After 80–90% confluency, H1 ESCs were dissociated with Accutase Cell Dissociation Reagent (Thermo Fisher Scientific, Madison, WI) for 4 min 30 s at room temperature, and then split at a ratio of ≈1:3 on Matrigel-coated plates (0.5 mg per 10 cm dish, Thermo Fisher Scientific). After culturing the cells for 2 d in E8BAC medium (E8 medium with Activin A (25 μg L^{-1}), BMP4 (5 μg L^{-1}), and CHIR 99021 (1 × 10^{-6} m)), the cells were cultured in E7Vi medium (E8 medium with VEGF-A (50 μg L^{-1}) and SB431542 (5 × 10^{-6} m; TGFβ inhibitor), but without TGFβ1) for 4 d. At harvest (day 6), differentiated ECs ($CD34^+$, $CD31^+$) were isolated with CD34 microbeads by MACS bead separation (Miltenyi Biotec, San Diego, CA). Isolated $CD34^+$ cells were cultured on Matrigel-coated plates in E7V medium (E8 medium with VEGF-A (50 μg L^{-1}), but without TGFβ1) for one passage before cryopreservation. A portion of live, harvested $CD34^+$ cells underwent flow cytometric analysis to verify that cells were >90% double positive for both CD34 and CD31 surface markers.

Primary human brain vascular pericytes (ScienCell Research Laboratories, Carlsbad, CA) were cultured according to manufacturer's instructions and maintained in pericyte medium (ScienCell Research Laboratories). Pericytes were used within four passages for all experiments.

PEG Hydrogel Fabrication

The synthetic PEG hydrogel formulation used for the encapsulation of ECs and pericytes was adapted from previous publications in our laboratory.[10,16]

At day 6 of culture, ECs were detached using Accutase treatment for 3–4 min at 37 °C, followed by 3–5 min centrifugation at 300 ×*g*. Pericytes were detached using 0.25% trypsin (ScienCell Research Laboratories) for 7–8 min at 37 °C, followed by 5 min centrifugation at 188 ×*g*. ECs (3400 cells μL^{-1}) and pericytes (1700 cells μL^{-1}) were resuspended in photoinitiator solution (0.1% I2959) in PBS and added 1:1 to a 2× PEG/peptide monomer solution. The final solution was pipetted into 24-well transwell inserts (Corning Falcon, 1 μm pores, 40 μL per insert) and polymerized for 4 min under a UV lamp (365 nm, 5–10 mW cm^{-2}, UVP XX-15L, Fisher). The polymerized gels were then immersed in E7V medium supplemented with 1× nonessential amino acids (Thermo Fisher Scientific) and 1× Glutamax (Thermo Fisher Scientific) for the duration of the experiment (1 mL under transwell, 200 μL in transwell).

Bioreactors for Dynamic Culture Conditions—Sterilization and Assembly of Bioreactors

The recirculating flow and continuous flow bioreactor top plates (CN Bio Innovations, Welwyn Garden City, England) were i) immersed in 10% bleach for ≥30 min, ii) thoroughly rinsed in deionized (DI) water to remove residual bleach, iii) immersed in 1% 7× detergent (MP Biomedicals, Santa Ana, CA) and sonicated at 60 Hz for 15 min, iv) thoroughly rinsed in DI water to remove residual detergent, v) immersed in DI water for 15 min with sonication twice, vi) allowed to air dry, vii) sealed in autoclavable pouches, and viii) autoclaved with a 45 min sterilization cycle followed by a 25 min drying cycle. After this sterilization process, the bottom (nonsterile) and sterile top plates of the bioreactors were assembled with sterile gaskets under sterile conditions and connected to air hoses and an air pump.

Bioreactors for Dynamic Culture Conditions—Culturing Vascular Networks in Bioreactors

Encapsulated ECs and pericytes were allowed to self-assemble and stabilize in 200 μL E7V medium for 1 d to allow for hydrogel swelling and to allow cells to stabilize and adhere to their surrounding matrix. After 24 h, transwells were transferred to bioreactors for dynamic flow or maintained as a static control (no flow). In the recirculating flow bioreactor, 1 mL medium was added to all wells underneath the transwell (Figure 1A). In the continuous flow bioreactor, 5 mL of E7V medium was added in the media reservoir (Figure 1B) with 1 mL medium added to the culture well underneath the transwell. Air pumps (CN Bio Innovations, Welwyn Garden City, England) derived the flow rate of 1 $\mu L\ s^{-1}$ underneath the transwell in both bioreactors (Figure 1). The flow rate in the input/feed media reservoir in the continuous flow bioreactor was adjusted to 0.006 $\mu L\ s^{-1}$, which provided 0.5 mL of fresh medium from the feeder reservoir to the center culture well each day (Figure 1B). In both the static

condition and recirculating flow bioreactor, medium was replaced every other day during culture. To avoid displacing the hydrogel, the medium inside the transwells in both bioreactors was not changed. After day 6 of culture, these samples were assessed with one of the following: i) autofluorescence multiphoton microscopy, ii) immunocytochemistry and confocal microscopy, or iii) scanning electron microscopy (Figure 1C).

Immunocytochemistry and Confocal Microscopy—Immunocytochemistry

After 6 d of culture, PEG hydrogels with embedded ECs and pericytes were fixed with 4% PFA for 2 h. Samples were then washed three times with 1× PBS for 5 min, followed by blocking and permeabilization with 0.25% Triton X-100 plus 10% donkey serum (DS) in PBS for 1 h, and then incubated in primary antibody solution (1% DS, 0.25% Triton X-100, 1% bovine serum albumin (BSA) in 0.01 m PBS) at the indicated dilutions overnight at 4 °C. Samples were washed three times with 0.01 m PBS for 30 min, incubated in secondary fluorescent antibody solution (1% DS, 0.25% Triton X-100, 1% BSA in PBS) for 2 h at room temperature, and then washed three times with 0.01 m PBS for 30 min. These fixed vascular networks were kept intact and in PBS during confocal imaging.

Immunocytochemistry and Confocal Microscopy—Antibodies

Antibodies and their commercial sources were as follows: anti-CD31 (Agilent Technologies, Santa Clara, CA; M0823, 1:200 dilution), anti- VE-cadherin (R&D Systems, Minneapolis, MN; AF938, 1:200 dilution), anti-PDGFRβ (Cell Signaling, 3169, 1:200 dilution), anti-αSMA (Abcam, Cambridge, MA; ab124964, 1:200 dilution), anti-ZO1 (Thermo Fisher Scientific; 40–2200, 1:100 dilution), donkey anti-rabbit Alexa-Fluor 568, donkey anti-mouse Alexa-Fluor 488, and donkey anti-goat Alexa-Fluor 647 (1:200 dilution, Thermo Fisher Scientific).

Immunocytochemistry and Confocal Microscopy—Confocal Imaging

A Nikon A1 confocal microscope was used to image the vascular networks after immunocytochemistry. Excitation wavelengths used were 488, 568, and 647 nm laser lines with corresponding emission filters of 525/50, 595/50, and >700 nm (long-pass), respectively. Volumes were acquired with either a 10× objective (NA 0.3, WD 16.0 mm, Nikon) or a 20× objective (NA 0.75, WD 1.0 mm, Nikon). The pinhole size was 1.2 Airy units. Theoretical lateral/axial resolution with the 10× objective was 700 nm/10.86 μm at 525 nm, 793 nm/12.31 μm at 595 nm, and 953 nm/14.79 μm at 715 nm. Theoretical lateral/axial resolution with the 20× objective was 280 nm/1.74 μm at 525 nm, 793 nm/1.97 μm at 595 nm, and 953 nm/2.37 μm at 715 nm. Calculation for axial resolution assumed sample refractive index of 1.33.

Dimensions for 10× volumes were 1024 × 1024 × 60 pixels with a voxel size of 1.27 μm × 5 μm (lateral × axial). Final spatial dimensions for 10× volumes were 1273 μm × 1273 μm × 300 μm (*x, y, z*). Dimensions of 20× volumes were 1024 × 1024 × 60 pixels with a voxel size of 635 nm × 5 μm (lateral × axial). Final spatial dimensions for 20× volumes were 637 μm × 637 μm × 300 μm (*x, y, z*). For visualization, MIPs were created for representative volumes. For quantification, MIPs were created from volumes stained for CD31 and imaged with the 10× objective.

Autofluorescence Multiphoton Microscopy Imaging

A multiphoton microscope (Bruker/Prairie Technologies, Madison, WI) was used to image the vascular networks. A Ti:Sapphire laser (Insight DS, Spectra-Physics, Santa Clara, CA) was intensity modulated with an electro-optic modulator (ConOptics, Danbury, CT), tuned to 750 nm, and coupled into an inverted microscope (Eclipse Ti-E, Nikon). A 20× air objective (NA 0.75, WD 1.0 mm, Nikon) focused the light into the sample. The theoretical lateral/axial resolution was 431 nm/2.66 μm at 750 nm. The calculation for axial resolution assumed a sample refractive index of 1.33. Emitted autofluorescence was collected with a bandpass filter centered at 440 (400–480 nm, Chroma, Bellows Falls, VT) and detected with a GaAsP photomultiplier tube (Hamamatsu, Japan) in a non-descanned configuration. The two-photon excitation/emission wavelengths were chosen to preferentially select for the fluorescence of NAD(P)H.[22,43]

For imaging, each transwell insert was removed from a multiwell plate and a custom stabilizing ring was fitted around the transwell. To minimize a mismatch in refractive index, a small volume of medium (100–150 μL) was transferred from the well onto the bottom of a 35 mm glass bottom dish (MatTek, Ashton, MA) and the transwell was placed with its porous membrane submerged in the medium.

3D volume mosaics were captured comprising either 3 × 5 × 50 or 4 × 4 × 50 frames (x, *y, z*) with each frame containing 512 × 512 pixels at a voxel size of 2.3 μm × 4 μm (lateral × axial). Final spatial dimensions of total 3D volume mosaic after image fusion[44] (ImageJ) were 1500 μm × 2550 μm × 200 μm and 2040 μm × 2040 μm × 200 μm (*x, y, z*), respectively. Pixel dwell time was 4.8 μs and each frame was averaged eight times.

Image Processing and Analysis—Segmentation

The image processing workflow is outlined in Figure 3. Our goal was to accurately segment the vascular network and quantify parameters of vascular network morphology. A maximum intensity projection of each 3D volume mosaic in the *z*-direction was created and background subtracted by first estimating the background by Gaussian blurring with a 200 μm × 200 μm kernel and then subtracting the estimated background from the image. Anisotropic diffusion filtering was applied to reduce noise in the image while preserving edge features.[45] The intensity of the vascular network varied over the maximum intensity projection, so CLAHE was used to locally increase the contrast between vessels and background *(adapthisteq,* MATLAB). This segmentation was refined to remove free cells from the image. Briefly, each connected region in the segmented image was filtered to remove regions containing less than nine connected pixels. For each remaining region, circularity, *C,* and eccentricity, *E,* were calculated. Circularity is defined as $C = 4\pi A/P^2$, where A is the area of the region and P is its perimeter. Eccentricity (E) measures the ratio of major axis length to minor axis length of an ellipse. A threshold of $C > 0.5$ and $E > 0.9$ allowed reliable segmentation of free cells vs the vascular network. The vascular network was further enhanced using multiscale Hessian filtering.[46] Segmentation using Otsu's threshold (*multithresh, imquantize,* MATLAB) created a rough mask, which was refined using active contour segmentation (*activecontour,* MATLAB) to create the final vessel mask. Automatically generated masks were compared to manually segmented masks via the

Sorensen-Dice coefficient for $n = 3$ representative images *(dice,* MATLAB). Sorensen-Dice coefficient was used to measure the similarity of two images and it ranged from 0 (no overlap) to 1 (complete overlap).

Image Processing and Analysis—Quantification

Vascular network formation was quantitatively assessed by extracting the morphological parameters depicted in Figure 4 and defined in Table 1. One value per MIP was extracted. Each MIP was created from one mosaic volume as defined above.

These parameters were quantified from the final vessel masks using previously established algorithms based on binary morphological operations as follows:

- *Active area*: For aMPM, the active area was manually defined for each MIP. The active area contains regions with vascular network formation, but excludes inactive areas (i.e., areas in the MIP where no vessels have formed). Figure S3A in the Supporting Information shows a representative MIP with the active area in yellow and the inactive area in red. No dependence of the active area on culture condition was found (not significant, analysis of variance (ANOVA), data not shown). The MIPs for confocal microscopy did not contain inactive regions; thus, for confocal quantification, the active area was defined as the entire image area.
- *Vessel diameters*: A Euclidean distance transform (*bwdist,* MATLAB) was applied to the complemented binary vessel mask (vessels = 0; background = 1). Each pixel in the distance transformed image is the distance between that pixel and the nearest nonzero pixel; thus, pixels along the centerline of each vessel represent the radius of the vessel at that pixel. A skeleton of the final vessel mask was created (*bwmorph,* MATLAB) and multiplied with the distance transformed image to extract the vessel radii in pixels, which were converted to vessel diameters in units of micrometers.
- *Vascular density*: The area of the final vessel mask (all pixels of binary mask summed together) was normalized by the active area (Figure S3A, Supporting Information).
- *Branch point density*: A skeleton of the final vessel mask was created (*bwmorph,* MATLAB) and used to find the total number of branch points (*bwmorph,* MATLAB) in each MIP. This number was normalized by the active area (Figure S3A, Supporting Information).
- *Free/networked ratio*: The number of free cells was extracted from the binary mask generated during free cell removal, which selects for and removes free cells based on area, circularity, and ellipticity thresholds. Free cells can be found as single cells or arranged in small clusters of touching cells, so a standard algorithm was applied to also separate touching cells: i) Euclidean distance transform, ii) take complement, iii) H-minima transform, and iv) watershed transform. The number of free cells, including cells split from clusters, was

counted by standard morphological image processing (*bwconncomp,* MATLAB) and normalized by the area of the final vessel mask.

- *Network anisotropy*: Network anisotropy quantifies the overall alignment of vessels within a vascular network. The Fourier transform method is a validated method to extract the network anisotropy from an image, and is described in more detail elsewhere.[47] Briefly, the 2D power spectrum was calculated using the skeleton image for each vascular network. The skeleton image allowed assessment of the alignment of each vessel with every other vessel. Bandpass filtering was used to exclude the DC component and high-frequency noise. The power spectrum was then summed in 1° intervals, which captures the orientation of structures within the image. Projecting this 360 element vector into 2D allows us to form a second-rank orientation tensor. The network anisotropy is an angle-independent metric of the overall alignment of all structure within the image, and was calculated as follows: network anisotropy = $1 - \lambda_2/\lambda_1$, where λ_2 and λ_1 are second and first eigenvalues of the eigendecomposition of the orientation tensor, respectively.
- *Hardware*: All processing was performed using MATLAB (R2017b, 64-bit, MathWorks, Natick, MA) on a 64-bit Windows 10 workstation with an Intel Xeon quad-core processor (2.8 GHz, E5–1603) and 64GB of RAM.

SEM Imaging

Hydrogels containing vascular networks were immersed in a buffered solution of 2% PFA in 0.01 m PBS for 20 min, and then immersed in 1.5% glutaraldehyde in freshly prepared 70×10^{-3} m sodium cacodylate buffer, pH 7.4. The samples were then rinsed in 70×10^{-3} m sodium cacodylate buffer containing 2.5% sucrose and incubated at room temperature for 30 min. The dehydration was achieved by sequential immersion of samples in a graduated series of ethanol in H_2O and hexamethyldisilazane in 30%, 50%, 80%, and 95% ethanol. The samples were left to dry on the sample holder and then gold sputter coated prior to imaging with a scanning electron microscope (SEM LEO 1530).

Statistics

Data were presented as individual data points along with their mean ± standard error of the mean. Final sample sizes used for aMPM quantification included $n = 6$ replicates for static and continuous flow bioreactor and $n = 5$ replicates for the recirculating flow bioreactor. Final sample size for confocal microscopy quantification included $n = 3$ for all groups. One-way ANOVA tests followed by Tukey's honest significant difference test were performed using MATLAB. Statistical significance was defined as $P < 0.05$.

Supplementary Material

Refer to Web version on PubMed Central for supplementary material.

Acknowledgements

G.K. and D.A.G. contributed equally to this work. This research was supported by the National Institutes of Health (R01 HL093282-01A1, 1U H2TR000506-01, 3UH2TR000506-02S1, 4U H3TR000506-03, R01CA205101, R01CA185747, R01CA211082, R01CA226526), the National Science Foundation (CBET-1642287), and Stand Up To Cancer (SU2C-AACR-IG-08-16). This research was additionally supported by the Environmental Protection Agency STAR Center grant #835737. The authors thank the Department of Orthopedics, University of Wisconsin-Madison, and the Morgridge Institute for Research for providing all required support for this research. After initial online publication on December 19, 2018, M.C.S. was added to the fourth affiliation address. Figures 5 and 6 were initially uploaded in error, and new versions provided. This does not affect the conclusions of the results in this paper.

References

[1]. Belair DG, Whisler JA, Valdez J, Velazquez J, Molenda JA, Vickerman V, Lewis R, Daigh C, Hansen TD, Mann DA, Thomson JA, Griffith LG, Kamm RD, Schwartz MP, Murphy WL, Stem Cell Rev. Rep 2015, 11, 511.

[2]. Griffith CK, Miller C, Sainson RCA, Calvert JW, Jeon NL, Hughes CCW, George SC, Tissue Eng. 2005, 11, 257. [PubMed: 15738680]

[3]. Kolesky DB, Homan KA, Skylar-Scott MA, Lewis JA, Proc. Natl. Acad. Sci. USA 2016, 113, 3179. [PubMed: 26951646]

[4]. a)Marx V, Nature 2015, 522, 373 [PubMed: 26085275] b)Liu J, Zheng HY, Poh PSP, Machens HG, Schilling AF, Int. J. Mol. Sci 2015, 16, 15997. [PubMed: 26184185]

[5]. a)Carmeliet P, Jain RK, Nature 2000, 407, 249 [PubMed: 11001068] b)Jain RK, Au P, Tam J, Duda DG, Fukumura D, Nat. Biotechnol 2005, 23, 821. [PubMed: 16003365]

[6]. Tsang VL, Chen AA, Cho LM, Jadin KD, Sah RL, DeLong S, West JL, Bhatia SN, FASEB J. 2007, 21, 790. [PubMed: 17197384]

[7]. Nguyen EH, Zanotelli MR, Schwartz MP, Murphy WL, Biomaterials 2014, 35, 2149. [PubMed: 24332391]

[8]. Wang XY, Jin ZH, Gan BW, Lv SW, Xie M, Huang WH, Lab Chip 2014, 14, 2709. [PubMed: 24887141]

[9]. Datta P, Ayan B, Ozbolat IT, Acta Biomater. 2017, 51, 1. [PubMed: 28087487]

[10]. Zanotelli MR, Ardalani H, Zhang J, Hou ZG, Nguyen EH, Swanson S, Nguyen BK, Bolin J, Elwell A, Bischel LL, Xie AW, Stewart R, Beebe DJ, Thomson JA, Schwartz MP, Murphy WL, Acta Biomater. 2016, 35, 32. [PubMed: 26945632]

[11]. Vickerman V, Blundo J, Chung S, Kamm R, Lab Chip 2008, 8, 1468. [PubMed: 18818801]

[12]. Moya ML, Hsu YH, Lee AP, Hughes CCW, George SC, Tissue Eng., Part C 2013, 19, 730.

[13]. Folkman J, Haudenschild C, Nature 1980, 288, 551. [PubMed: 6160403]

[14]. Moon JJ, Saik JE, Poche RA, Leslie-Barbick JE, Lee SH, Smith AA, Dickinson ME, West JL, Biomaterials 2010, 31, 3840. [PubMed: 20185173]

[15]. a)Belair DG, Schwartz MP, Knudsen T, Murphy WL, Acta Biomater. 2016, 39, 12 [PubMed: 27181878] b)Nguyen EH, Daly WT, Le NNT, Farnoodian M, Belair DG, Schwartz MP, Lebakken CS, Ananiev GE, Saghiri MA, Knudsen TB, Sheibani N, Murphy WL, Nat. Biomed. Eng 2017, 1, 0096. [PubMed: 29104816]

[16]. Zhang J, Schwartz MP, Hou ZG, Bai YS, Ardalani H, Swanson S, Steill J, Ruotti V, Elwell A, Nguyen BK, Bolin J, Stewart R, Thomson JA, Murphy WL, Stem Cell Rep. 2017, 8, 907.

[17]. Schwartz MP, Hou ZG, Propson NE, Zhang J, Engstrom CJ, Costa VS, Jiang P, Nguyen BK, Bolin JM, Daly W, Wang Y, Stewart R, Page CD, Murphy WL, Thomson JA, Proc. Natl. Acad. Sci. USA 2015, 112, 12516. [PubMed: 26392547]

[18]. Ruan JL, Tulloch NL, Muskheli V, Genova EE, Mariner PD, Anseth KS, Murry CE, Tissue Eng., Part C 2013, 19, 794.

[19]. Kalyanaraman B, Zielonka J, Redox Biol. 2017, 12, 755. [PubMed: 28415040]

[20]. Skala MC, Riching KM, Gendron-Fitzpatrick A, Eickhoff J, Eliceiri KW, White JG, Ramanujam N, Proc. Natl. Acad. Sci. USA 2007, 104, 19494. [PubMed: 18042710]

[21]. Hoover EE, Squier JA, Nat. Photonics 2013, 7, 93. [PubMed: 24307915]

[22]. a)Shah AT, Diggins KE, Walsh AJ, Irish JM, Skala MC, Neoplasia 2015, 17, 862 [PubMed: 26696368] b)Walsh AJ, Cook RS, Sanders ME, Aurisicchio L, Ciliberto G, Arteaga CL, Skala MC, Cancer Res. 2014, 74, 5184. [PubMed: 25100563]

[23]. Helm CLE, Zisch A, Swartz MA, Biotechnol. Bioeng 2007, 96, 167. [PubMed: 17133613]

[24]. Shields JD, Fleury ME, Yong C, Tomei AA, Randolph GJ, Swartz MA, Cancer Cell 2007, 11, 526. [PubMed: 17560334]

[25]. Wong AP, Perez-Castillejos R, Love JC, Whitesides GM, Biomaterials 2008, 29, 1853. [PubMed: 18243301]

[26]. a)Kleinstreuer NC, Judson RS, Reif DM, Sipes NS, Singh AV, Chandler KJ, DeWoskin R, Dix DJ, Kavlock RJ, Knudsen TB, Environ. Health Perspect 2011, 119, 1596 [PubMed: 21788198] b)Knudsen TB, Kleinstreuer NC, Birth Defects Res., Part C 2011, 93, 312c)Kleinstreuer N, Dix D, Rountree M, Baker N, Sipes N, Reif D, Spencer R, Knudsen T, PLoS Comput. Biol 2013, 9, e1002996. [PubMed: 23592958]

[27]. Orlova VV, Drabsch Y, Freund C, Petrus-Reurer S, van den Hil FE, Muenthaisong S, Dijke PT, Mummery CL, Arterioscler. Thromb. Vasc. Biol 2014, 34, 177. [PubMed: 24158517]

[28]. Orlova VV, van den Hil FE, Petrus-Reurer S, Drabsch Y, Ten Dijke P, Mummery CL, Nat. Protoc 2014, 9, 1514. [PubMed: 24874816]

[29]. Harris ES, Nelson WJ, Curr. Opin. Cell Biol 2010, 22, 651. [PubMed: 20708398]

[30]. McMurtrey RJ, Stem Cells Dev. 2017, 26, 1293. [PubMed: 28707964]

[31]. Yin X, Mead BE, Safaee H, Langer R, Karp JM, Levy O, Cell Stem Cell 2016, 18, 25. [PubMed: 26748754]

[32]. Kusuma S, Shen YI, Hanjaya-Putra D, Mali P, Cheng LZ, Gerecht S, Proc. Natl. Acad. Sci. USA 2013, 110, 12601. [PubMed: 23858432]

[33]. a)Geevarghese A, Herman IM, Transl. Res 2014, 163, 296 [PubMed: 24530608] b)Wang SJ, Cao CH, Chen ZM, Bankaitis V, Tzima E, Sheibani N, Burridge K, PLoS One 2012, 7, e45499 [PubMed: 23029055] c)Stratman AN, Davis GE, Microsc. Microanal 2012, 18, 68. [PubMed: 22166617]

[34]. Baluk P, Fuxe J, Hashizume H, Romano T, Lashnits E, Butz S, Vestweber D, Corada M, Molendini C, Dejana E, McDonald DM, J. Exp. Med 2007, 204, 2349. [PubMed: 17846148]

[35]. Berardi DE, Tarbell JM, Cell. Mol. Bioeng 2009, 2, 320. [PubMed: 20161517]

[36]. Perdiguero EG, Galaup A, Durand M, Teillon J, Philippe J, Valenzuela DM, Murphy AJ, Yancopoulos GD, Thurston G, Germain S, J. Biol. Chem 2011, 286, 36841. [PubMed: 21832056]

[37]. a)Chen LC, Lloyd WR, Kuo S, Kim HM, Marcelo CL, Feinberg SE, Mycek MA, Biomaterials 2014, 35, 6667 [PubMed: 24854093] b)Sobrino A, Phan DTT, Datta R, Wang XL, Hachey SJ, Romero-Lopez M, Gratton E, Lee AP, George SC, Hughes CCW, Sci. Rep 2016, 6, 31589 [PubMed: 27549930] c)Quinn KP, Bellas E, Fourligas N, Lee K, Kaplan DL, Georgakoudi I, Biomaterials 2012, 33, 5341 [PubMed: 22560200] d)Ward A, Quinn KP, Bellas E, Georgakoudi I, Kaplan DL, PLoS One 2013, 8, e55696 [PubMed: 23405199] e)Syverud BC, Mycek MA, Larkin LM, Tissue Eng., Part C 2017, 23, 616.

[38]. Horton NG, Wang K, Kobat D, Clark CG, Wise FW, Schaffer CB, Xu C, Nat. Photonics 2013, 7, 205.

[39]. Smith Q, Gerecht S, Curr. Opin. Chem. Eng 2014, 3, 42. [PubMed: 24644533]

[40]. Mahou P, Vermot J, Beaurepaire E, Supatto W, Nat. Methods 2014, 11, 600. [PubMed: 24874570]

[41]. a)Haft-Javaherian M, Fang L, Muse V, Schaffer CB, Nishimura N, Sabuncu MR, arXiv: 1801.00880v3 [cs.CV] 2018b)Bates R, Irving B, Markelc B, Kaeppler J, Brown G, Muschel RJ, Brady SM, Grau V, Schnabel JA, IEEE Transactions on Medical Imaging 2018, 1 [PubMed: 28945591] c)Almasi S, Ben-Zvi A, Lacoste B, Gu CH, Miller EL, Xu XY, Pattern Recognit. 2017, 63, 710. [PubMed: 28566796]

[42]. Shen N, Riedl JA, Berrio DAC, Davis Z, Monaghan MG, Layland SL, Hinderer S, Schenke-Layland K, Biomed. Mater 2018, 13, 024101. [PubMed: 29148433]

[43]. a)Zipfel WR, Williams RM, Christie R, Nikitin AY, Hyman BT, Webb WW, Proc. Natl. Acad. Sci. USA 2003, 100, 7075 [PubMed: 12756303] b)Huang SH, Heikal AA, Webb WW, Biophys. J 2002, 82, 2811. [PubMed: 11964266]

[44]. Preibisch S, Saalfeld S, Tomancak P, Bioinformatics 2009, 25, 1463. [PubMed: 19346324]

[45]. Kroon D-J, Image edge enhancing coherence filter toolbox, http://www.mathworks.com/matlabcentral/fileexchange/25449-image-edge-enhancing-coherence-filter-toolbox, (accessed: May).

[46]. a)Kroon D-J, Hessian based Frangi vesselness filter, http://www.mathworks.com/matlabcentral/fileexchange/24409-hessian-based-frangi-vesselness-filter, (accessed: October 2017)b)Frangi AF, Niessen WJ, Vincken KL, Viergever MA, Medical Image Computing and Computer-Assisted Intervention—Miccai'98, Vol. 1496, Cambridge, MA, USA 1998, p. 130.

[47]. Sander EA, Barocas VH, J. Biomed. Mater. Res., Part A 2009, 88A, 322.

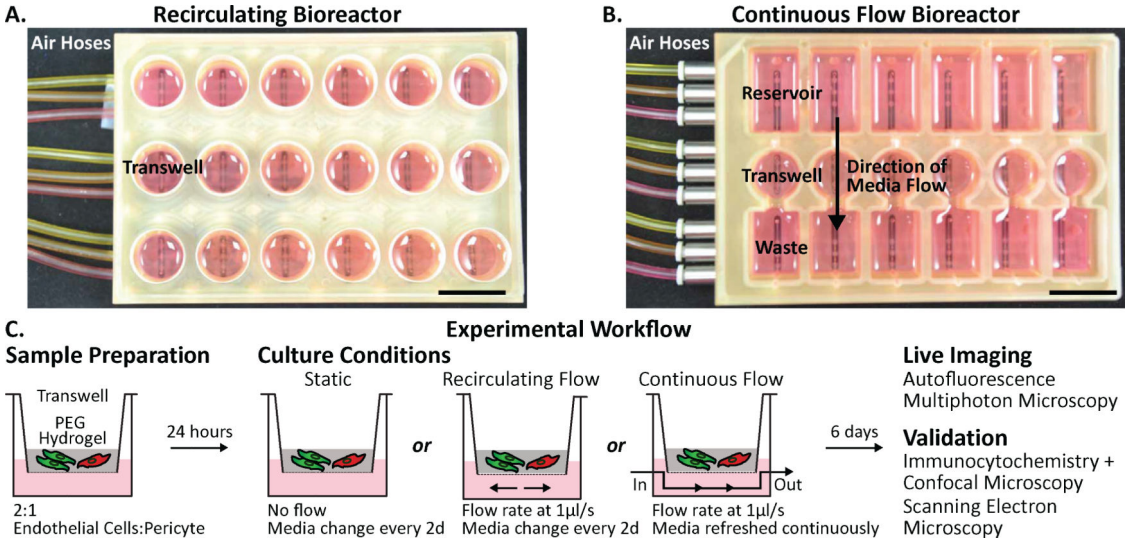

Figure 1.

Overview of bioreactors and experimental workflow. Two bioreactors (CN Bio Innovations) were used to create dynamic culture conditions during vascular network formation. A) The recirculating bioreactor cultures up to 18 transwells simultaneously. Recirculating flow is generated using a sequence of air puffs beneath the nonporous membrane at the bottom of each well. B) The continuous flow bioreactor contains six wells, each with its own media reservoir and waste chamber. Continuous, unidirectional flow is generated by the pumping of media from the reservoir into the well, which expels waste media into the waste chamber. C) H1 embryonic stem cell–derived endothelial cells (green) and primary human pericytes (red) were seeded in a 2:1 ratio within a synthetic PEG hydrogel in a transwell insert. Vascular networks were cultured in three conditions: static, recirculating, and continuous flow. Both the recirculating and continuous flow bioreactors created flow beneath the transwell at a rate of 1 μL s^{-1}. Media in the static and recirculating cultures were changed every 2 d, while media were constantly refreshed in the continuous flow bioreactor. After 6 d of culture, each vascular network was assessed with one of the following: i) autofluorescence multiphoton microscopy, ii) immunocytochemistry + confocal microscopy, or iii) scanning electron microscopy.

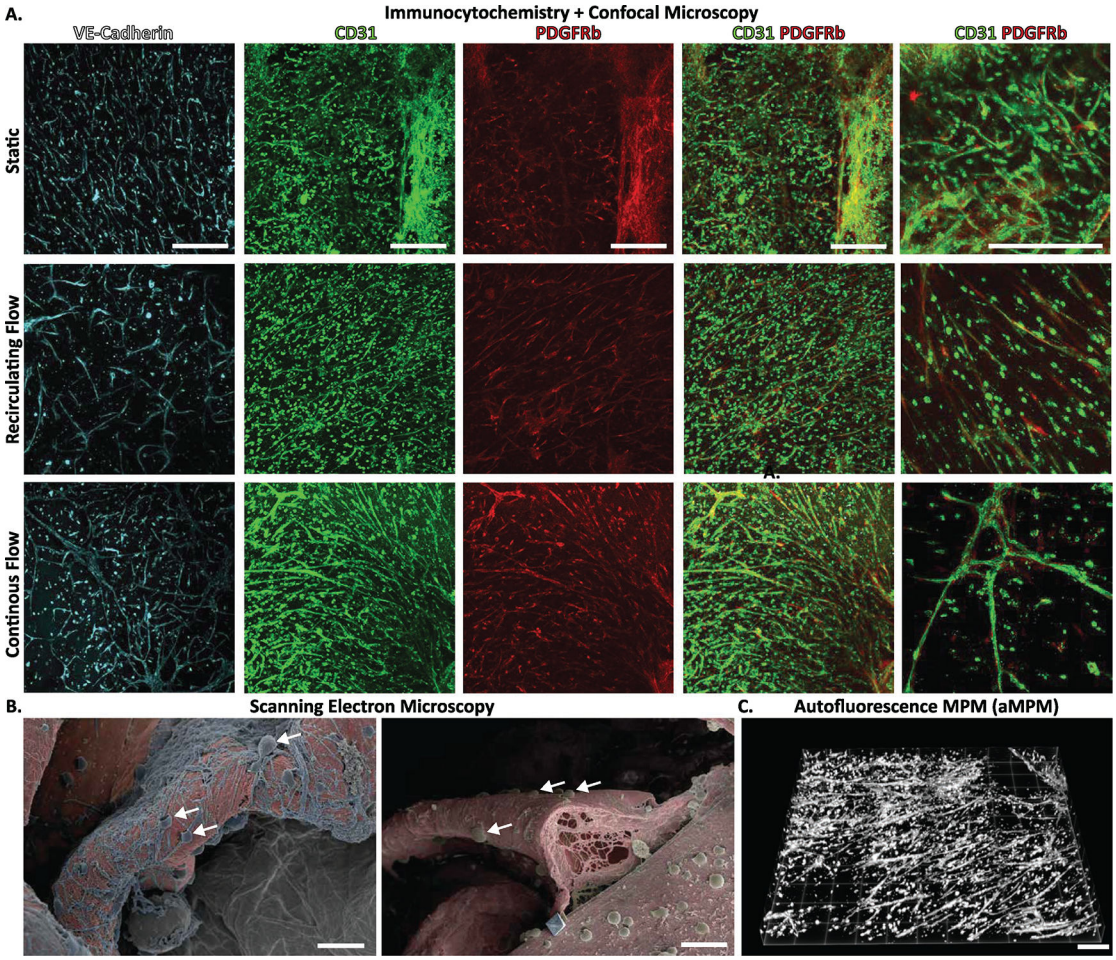

Figure 2.

Characterization of self-assembled vascular networks. A) At day 6, vascular network formation was characterized using standard fixation and immunofluorescence protocols. ECs were labeled based on VE-cadherin (Cy5, white) or CD31 expression (green) and pericytes were labeled based on PDGFRβ (red). Samples were imaged in 3D with confocal microscopy and displayed as MIPs. MIPs of CD31 and PDGFRβ expression showed colocalization of ECs and pericytes within vascular networks formed in all culture conditions. Last column represents the magnified regions (20× magnification) of the merged images from the fourth column. Scale bars: 300 μm. B) Color-enhanced SEM images showed the 3D vascular network at day 6, where ECs (red) and pericytes (grey) were colocalized. Pericytes (white arrows) wrap around the EC lumen. Scale bar: 1 μm. C) Rendering of aMPM volume shows the 3D morphology of self-assembled vascular networks. Scale bar: 400 μm.

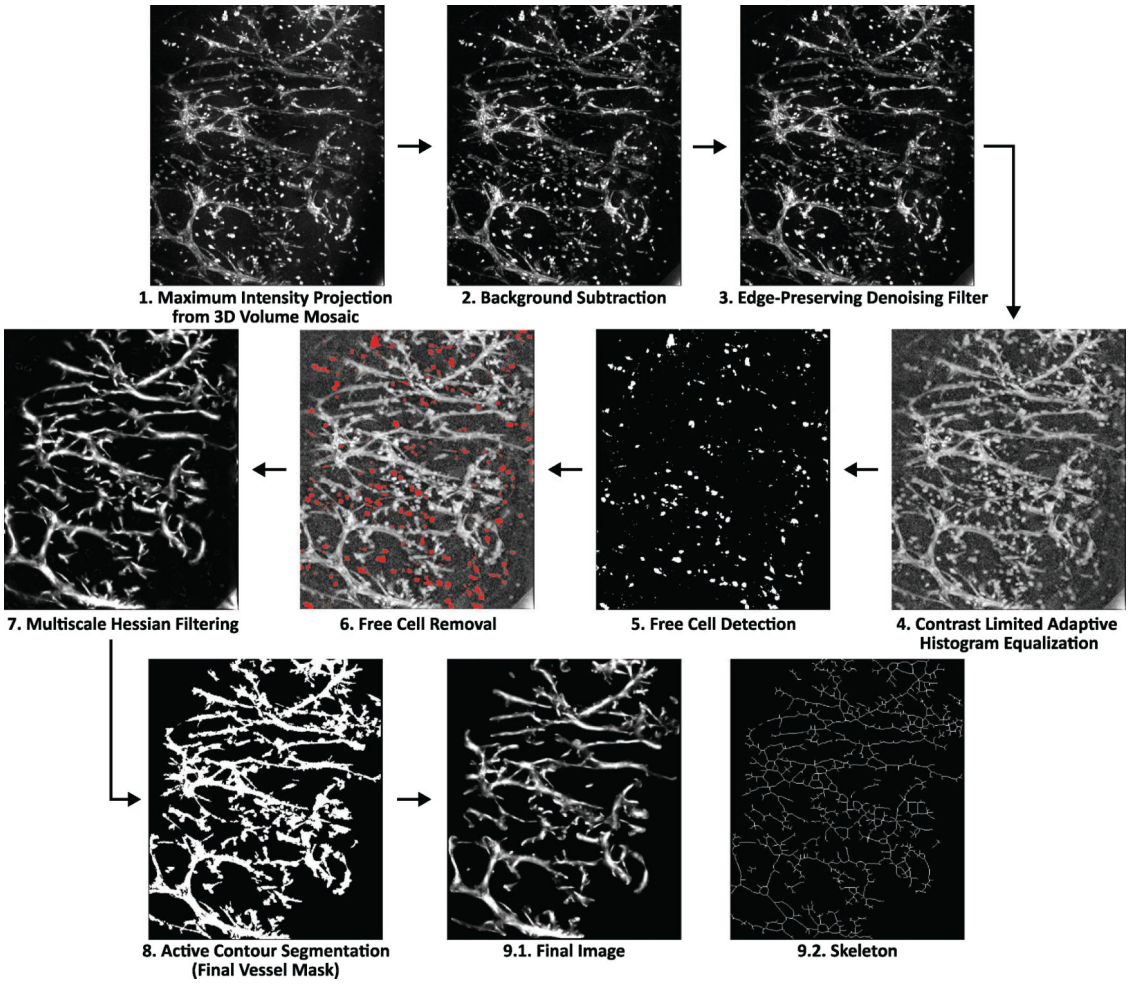

Figure 3.

Image processing for vascular segmentation of autofluorescence images. An image processing workflow was used to enhance the vascular network before quantification of morphological parameters: 1) A MIP was calculated from each 3D volume. 2) Background subtraction was used to correct for variations in background intensity across the MIP. 3) Anisotropic diffusion filtering was used to reduce noise while preserving edges. 4) CLAHE improved local contrast in the MIP to allow better segmentation for free cell detection and removal. 5) After segmentation, free cells were identified based on size, circularity, and ellipticity thresholding. 6) Free cells were removed from the image. 7) Multiscale Hessian filtering enhances vessel-like structures while suppressing other structures and noise in the image. 8) The final vessel mask used for quantification was created with active contour segmentation. 9.1) Final image was created by applying the final vessel mask to the multiscale Hessian filtered image. 9.2) Skeleton was made from the final vessel mask and used for quantification.

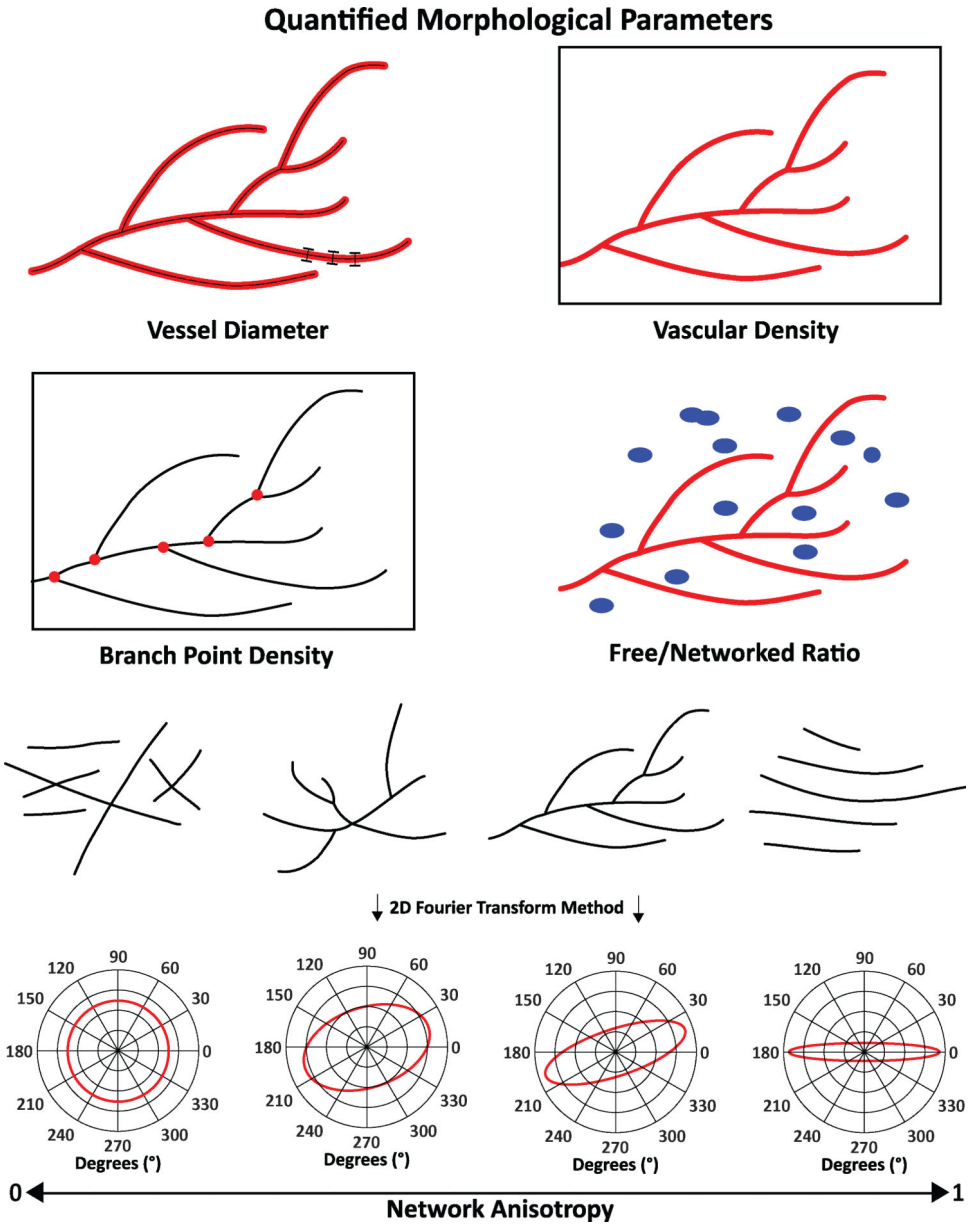

Figure 4.

Visual representation of quantified morphological parameters. Vascular network morphology was quantified by algorithms that operate on binary masks, which were generated from maximum intensity projections of image volumes. This visual representation provides intuition to aid in the interpretation of each of the following morphological parameters: vessel diameter, vascular density, branch point density, free/networked ratio, and network anisotropy. Specific definitions of how these parameters are calculated can be found in Table 1.

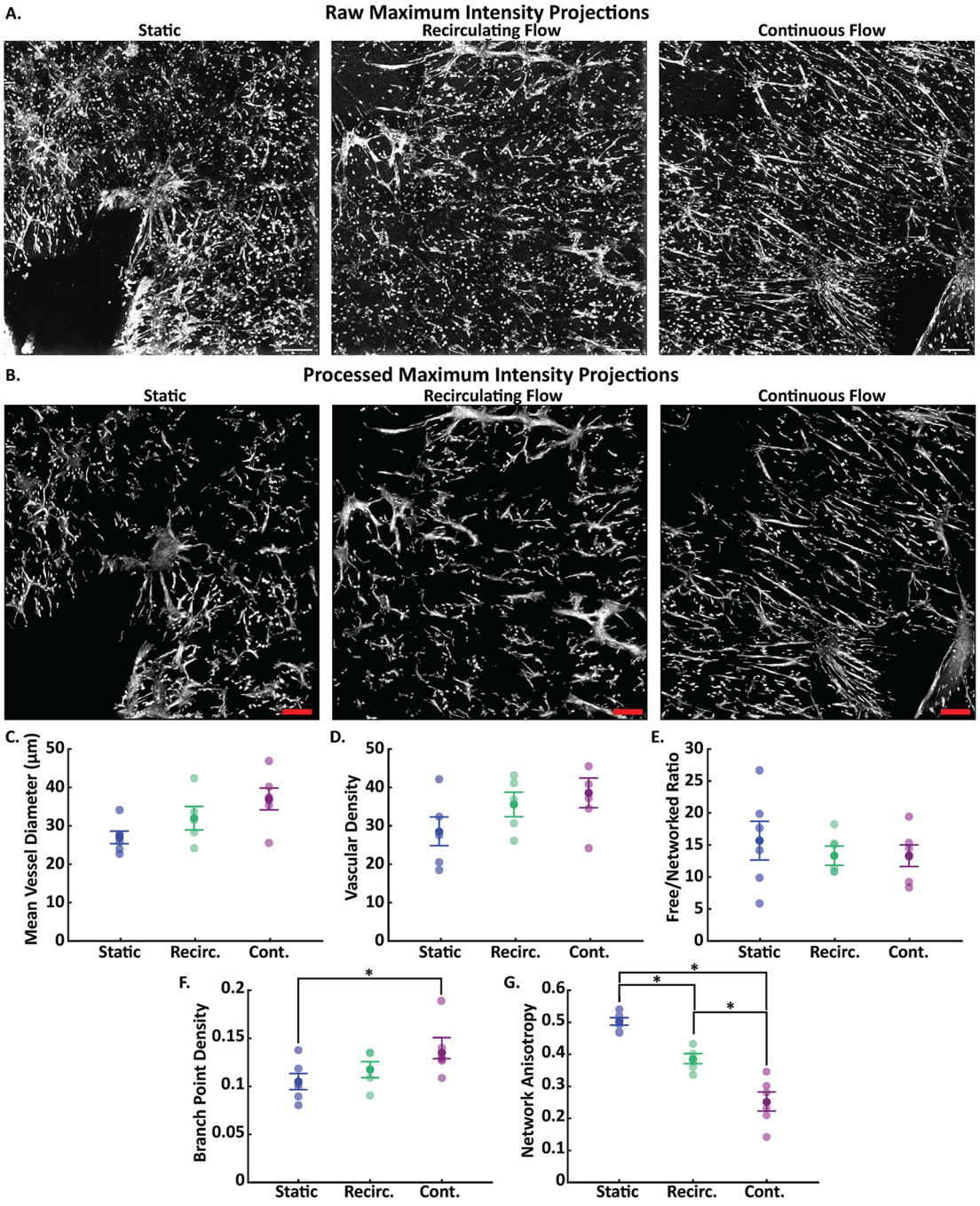

Figure 5.

Quantitative morphological analysis of autofluorescence multiphoton microscopy data. A) aMPM visualized the vascular networks without the need for fixation or exogenous fluorophores. Representative MIPs of aMPM volumes show formation of 3D vascular networks in all three conditions: static, recirculating, and continuous flow. Free, non-networked cells are distributed throughout the hydrogel. Scale bar: 200 μm. B) An image processing and analysis pipeline was developed to quantify vascular network morphology using MIPs of aMPM volumes. Representative processed MIPs demonstrate the

enhancement of vascular structures, removal of free cells, and suppression of background noise. Segmentation was performed on processed MIPs to create a binary mask for quantification. Scale bar: 200 μm. C-G) Parameters extracted from binary masks of MIPs quantitatively assessed the morphology of networks cultured under different culture conditions. Mean vessel diameter (C), vascular density (D), and free/networked ratio (E), a measure of cell integration into the network, were not significantly different across culture conditions. Continuous flow significantly increased branch point densities (F), compared to static culture, and lowered network anisotropy (G), compared to both static and recirculating cultures. Recirculating flow induced formation of vascular networks with decreased network anisotropy (G), compared to static culture. Data ($n = 6$ for static and continuous flow bioreactor and $n = 5$ for the recirculating flow bioreactor) are plotted as individual data points along with the mean ± standard error of the mean and analyzed using a one-way ANOVA followed by Tukey's honest significant difference post hoc test. Statistical significance is indicated by * for $P < 0.05$.

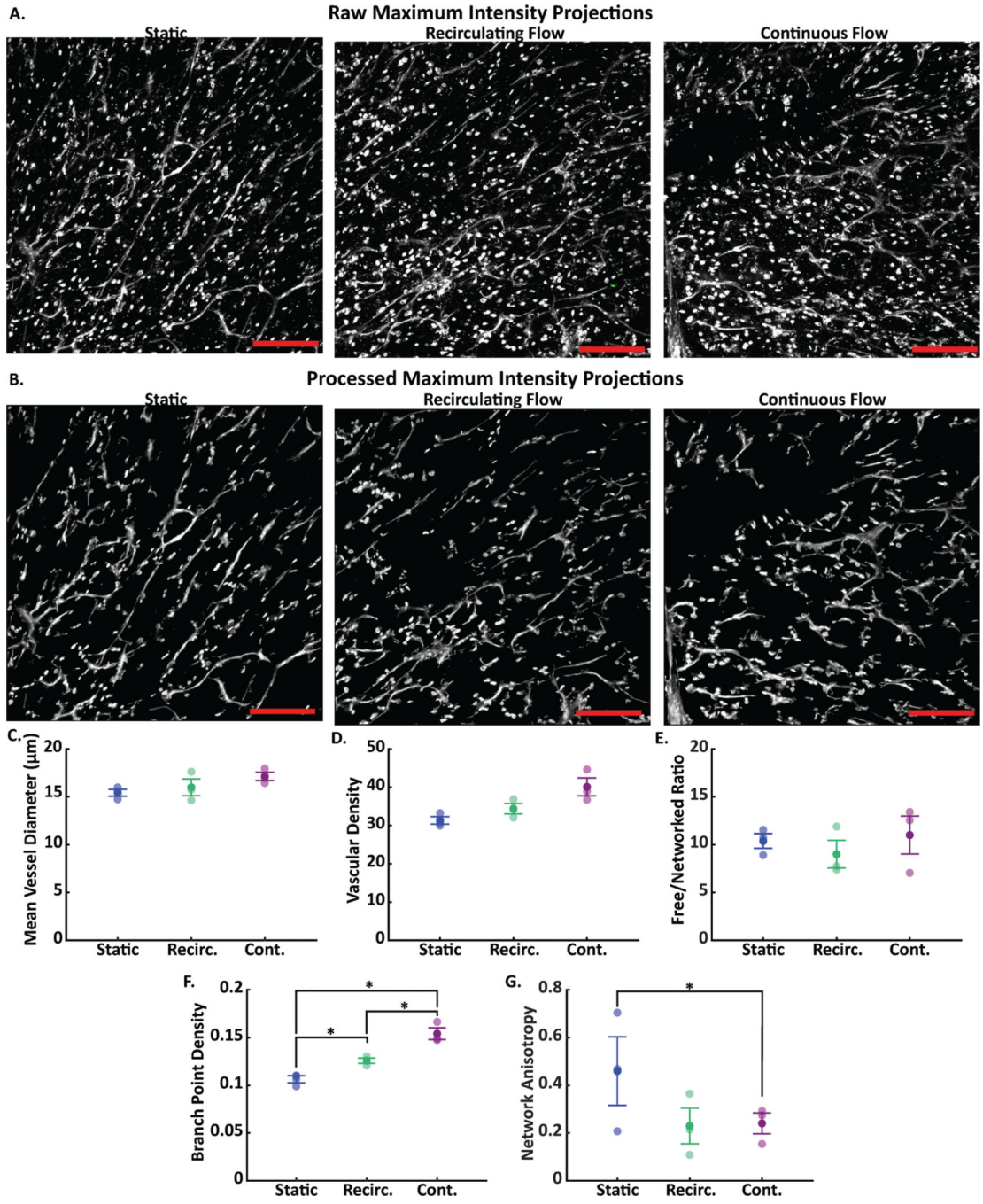

Figure 6.

Quantitative morphological analysis of immunocytochemistry data. A) Immunofluorescence and confocal microscopy were performed to visualize the vascular network by labeling CD31, a marker of endothelial cells. Representative MIPs show vascular networks cultured in three conditions: static, recirculating, and continuous flow. Free endothelial cells, i.e., not integrated into the vascular network, are observed throughout the hydrogel. Scale bar: 200 μm. B) The image processing and analysis pipeline developed to quantify aMPM MIPs was applied to confocal MIPs of fixed immunofluorescence samples. Representative processed

MIPs demonstrate the enhancement of vascular structures, removal of free cells, and suppression of background noise. Segmentation was performed on processed MIPs to create a binary mask for quantification. Scale bar: 200 μm. C-G) Morphological parameters extracted from confocal MIPs of fixed immunofluorescence samples. MIPs quantitatively assessed network formation under three culture conditions. Mean vessel diameter (C), vascular density (D), and free/networked ratio (E) were not significantly different across culture conditions. Continuous flow significantly increased branch point densities (F), compared to static culture and recirculating flow, and had lower network anisotropy (G) compared to both static conditions. Recirculating flow induced formation of vascular networks with increased branch point densities (F) compared to static culture. Data ($n = 3$) are plotted as individual data points along with the mean ± standard error of the mean and analyzed using a one-way ANOVA followed by Tukey's honest significant difference post hoc test. Statistical significance is indicated by * for $P < 0.05$.

Table 1.

Morphological parameters.

Parameter name	Definition
Vessel diameter	Distance across the lumen of each vessel averaged across all vessels per MIP
Vascular density	Total vessel area divided by active area
Branch point density	Number of branch points divided by active area
Free/networked ratio	Number of free cells divided by vessel area
Network anisotropy	1 - ratio of the minor-to-major axes of the 2D angle distribution of vessels within the vascular network (0 = fully random orientations; 1 = fully aligned)